ORIGINAL ARTICLE

CRH stimulation improves ^{18}F-FDG-PET detection of pituitary adenomas in Cushing's disease

Jacqueline Boyle[1,2] · Nicholas J. Patronas[3] · James Smirniotopoulos[4] · Peter Herscovitch[5] · William Dieckman[5] · Corina Millo[5] · Dragan Maric[6] · Grégoire P. Chatain[7] · Christina Piper Hayes[8] · Sarah Benzo[8] · Gretchen Scott[8] · Nancy Edwards[8] · Abhik Ray Chaudhury[8] · Maya B. Lodish[9] · Susmeeta Sharma[10] · Lynnette K. Nieman[11] · Constantine A. Stratakis[9] · Russell R. Lonser[12] · Prashant Chittiboina[1,8]

Abstract

Objective In MRI-negative cases Cushing's disease (CD), surgeons perform a more extensive exploration of the pituitary gland, with fewer instances of hormonal remission. ^{18}F-fluoro-deoxy-glucose (^{18}F-FDG) positron emission tomography (PET) has a limited role in detecting adenomas that cause CD (corticotropinomas). Our previous work demonstrated corticotropin-releasing hormone (CRH) stimulation leads to delayed, selective glucose uptake in corticotropinomas. Here, we prospectively evaluated the utility of CRH stimulation in improving ^{18}F-FDG-PET detection of adenomas in CD.

Methods Subjects with a likely diagnosis of CD ($n = 27$, 20 females) each underwent two ^{18}F-FDG-PET studies [without and with ovine-CRH (oCRH) stimulation] on a high-resolution PET platform. Standardized-uptake-values (SUV) in the sella were calculated. Two blinded neuroradiologists independently read ^{18}F-FDG-PET images qualitatively. Adenomas were histopathologically confirmed, analyzed for mutations in the *USP8* gene and for glycolytic pathway proteins.

Results The mean-SUV of adenomas was significantly increased from baseline (3.6 ± 1.5) with oCRH administration (3.9 ± 1.7; one-tailed $p = 0.003$). Neuroradiologists agreed that adenomas were visible on 21 scans, not visible on 26 scans (disagreed about 7, *kappa* = 0.7). oCRH-stimulation led to the detection of additional adenomas ($n = 6$) not visible on baseline-PET study. Of the MRI-negative adenomas ($n = 5$), two were detected on PET imaging (one only after oCRH-stimulation). *USP8* mutations or glycolytic pathway proteins were not associated with SUV in corticotropinomas.

✉ Prashant Chittiboina
 prashant.chittiboina@nih.gov

1 Neurosurgery Unit for Pituitary and Inheritable Diseases, National Institute of Neurological Diseases and Stroke, Bethesda, MD, USA

2 University of Illinois College of Medicine at Peoria, Peoria, IL, USA

3 Diagnostic Radiology, Warren Grant Magnuson Clinical Center, National Institutes of Health, Bethesda, MD, USA

4 Department of Radiology, George Washington University, Washington, DC, USA

5 Department of Positron Emission Tomography, Warren Grant Magnuson Clinical Center, National Institutes of Health, Bethesda, MD, USA

6 Flow Cytometry Core Facility, National Institute of Neurologic Diseases and Stroke, Bethesda, MD, USA

7 Surgical Neurology Branch, National Institute of Neurological Disorders and Stroke, Bethesda, MD, USA

8 Department of Neurosurgery, University of Colorado, Denver, CO, USA

9 Section on Endocrinology and Genetics, Pediatric Endocrinology Inter-Institute Training Program, Eunice Kennedy Shriver National Institute of Child Health and Human Development, Bethesda, MD, USA

10 Pituitary Endocrinology Section, MedStar Washington Hospital Center, Washington, DC, USA

11 Diabetes, Endocrinology and Obesity Branch, National Institute of Diabetes and Digestive and Kidney Diseases, Bethesda, MD, USA

12 Department of Neurological Surgery, The Ohio State University, Columbus, OH, USA

Conclusions The results of the current study suggest that oCRH-stimulation may lead to increased ^{18}F-FDG uptake, and increased rate of detection of corticotropinomas in CD. These results also suggest that some MRI invisible adenomas may be detectable by oCRH-stimulated FDG-PET imaging.

Clinical trial information ^{18}F-FDG-PET imaging with and without CRH stimulation was performed under the clinical trial NIH ID 12-N-0007 (clinicaltrials.gov identifier NCT01459237). The transsphenoidal surgeries and post-operative care was performed under the clinical trial NIH ID 03-N-0164 (clinicaltrials.gov identifier NCT00060541).

Keywords Pituitary adenoma · PET imaging · Cushing's disease · Transsphenoidal surgery · CRH · Secretagogue

Introduction

Accurate pre-operative localization of pituitary micro-adenomas in Cushing's disease (CD) leads to improved remission rates, and fewer adverse events following surgical adenoma extirpation [1, 2]. Modern MRI modalities including dynamic or volumetric sequences can reliably detect corticotroph adenomas in 50–80% cases of CD [3–7]. Patients with negative MRIs or lesions smaller than 6 mm undergo inferior petrosal sinus sampling (IPSS) to confirm a pituitary source of adrenocorticotropic hormone (ACTH) dependent hypercortisolemia [8, 9]. IPSS, however, does not improve tumor localization within the pituitary parenchyma for surgical planning [10]. In MRI negative cases, distinct adenomas are identified less commonly during surgery [7], leading to a more extensive exploration of the pituitary gland [11, 12]. Surgeons frequently perform more invasive surgeries such as hemihypophysectomy [8] or sub-total hypophysectomy to improve the chances of remission in these instances [12, 13].

Complementary imaging strategies are needed to improve detection of microadenomas in CD. Radioactive ^{18}F tagged fluoro-deoxy glucose (^{18}F-FDG) positron emission tomography (PET) often demonstrates increased glucose uptake in non-functioning and hormone secreting pituitary adenomas [14, 15], and minimal ^{18}F-FDG uptake in the normal pituitary gland [16–18]. While sellar ^{18}F-FDG uptake is highly specific [17–19], it is not sensitive for pituitary adenomas [3, 20]. We have previously shown that ^{18}F-FDG PET imaging can detect up to 40% corticotropinomas, some as small as 3 mm. We then asked if the rate of PET detection of corticotropinomas can be increased by secretagogue stimulation.

Using in vitro and ex vivo modeling, we have previously demonstrated that corticotropin-releasing hormone (CRH) stimulation leads to delayed glucose uptake (2–4 h) through increased glucose transporter 1 (GLUT1) transcription and membrane translocation in human corticotropinomas [21]. Here we evaluate the clinical applicability of these findings. We prospectively compared ^{18}F-FDG-PET findings in CD patients with and without ovine CRH (oCRH) stimulation.

Methods

Study design

The National Institute of Neurological Diseases and Stroke (NINDS) Combined Institutional Review Board approved the study (NINDS Study ID 12-N-0007, clinicaltrials.gov registration no. NCT01459237). The study was designed to evaluate the effect of oCRH stimulation on ^{18}F-FDG-PET imaging of corticotropinomas. The study was conducted between 2012 and 2018 at the National Institutes of Health Clinical Center, Bethesda, with an accrual ceiling of 30 subjects. Inclusion criteria included biochemical evidence of ACTH-dependent hypercortisolism (see below). The subjects also received standard pre-operative MRI of the pituitary gland with gadolinium contrast prior to inclusion in the study (see below). For this study, the subjects served as their own controls, with each receiving two ^{18}F-FDG-PET studies (one with oCRH stimulation), more than 24 h apart. Informed consent was obtained from all subjects or guardians (in the case of minors) prior to study participation. Initially, the study was designed for the subjects to undergo baseline PET and oCRH stimulated PET studies in random order, with CRH administered simultaneously with ^{18}F-FDG. However, we discovered convincing biological evidence for a delayed increase in glucose uptake following oCRH stimulation in corticotropinomas [21]. Following an interim analysis for safety after the 10th subject, the NINDS IRB approved a modification to introduce a delay of 2 and 4 h between oCRH and ^{18}F-FDG infusions.

CD diagnosis

Hypercortisolism was diagnosed on the basis of elevations of 24-h urine free cortisol (high performance liquid chromatography/tandem mass spectrometry: normal range: 2.6–37 μg/24 H for 9–12 year-olds, 4.0–56 μg/24 H for 13–17 year-olds and 3.5–45.0 μg/24 H for ≥18 year-olds), low-dose dexamethasone suppression testing (1 mg overnight or 2 mg over 48 h) [22], midnight serum cortisol (normal range < 7.5 mcg/dL) and/or 24-h urinary 17- hydroxycorticosteroids (17-OHS/Cr) excretion (2007—current Quest Diagnostics Nichols

Institute, Chantilly VA; normal range 3–10 mg/24 H for males and 2–6 mg/24 H for females).

Pituitary source of ACTH was determined by normal or increased morning plasma ACTH levels (Nichols Advantage Immunochemiluminometric assay or chemilumines-cence immunoassay, Siemens Immulite 2500 analyzer, NIH Department of Laboratory Medicine, Bethesda MD. 2005–2015 normal range 0.0–46.0 pg/mL; 2015—current normal range 5–46 pg/mL), 8 mg overnight dexamethasone suppression testing (DST), and ovine CRH stimulation testing. High resolution (1–1.5 mm slice thickness) magnetic resonance imaging (MRI) of the pituitary was performed to identify adenomas using T1 spin-echo and spoiled gradient recalled (3D-GRE) acquisition sequences [23]. The images were reviewed and reported as per standard of care (by on call neuroradiologists). Confirmatory IPSS was performed if biochemical data was incongruent or if MRI was non-diagnostic (MRI negative or lesions <6 mm).

Surgical procedure

The transsphenoidal surgeries and post-operative care was performed under the clinical trial NIH ID 03-N-0164 (clinicaltrials.gov identifier NCT00060541). A sublabial transsphenoidal surgery was performed on all patients included in this study [12, 13]. Briefly, wide exposure of the dura overlying sella and medial cavernous sinuses was performed following initial approach to the sella. Wide dural opening including medial cavernous sinuses was performed while preserving the underlying pituitary capsule. If an apparent 'adenoma' was evident on surface, circumferential dissection along the pseudocapsular plane was performed to remove the lesion en-bloc. In cases of cavernous sinus invasion, the involved medial wall of the cavernous sinus was removed. All surgical specimens underwent routine hematoxylin and eosin, reticulin staining, and ACTH immunostaining to confirm the diagnosis of corticotroph adenoma. In instances where an exploration of the sella with multiple specimens were procured, each specimen was labeled for its site including elevation and laterality within the sella.

^{18}F-FDG-PET image acquisition

PET imaging was performed using a high-resolution research tomography scanner (Siemens AG; Erlangen, Germany) as previously reported [3]. Briefly, subjects were asked to fast (except water) for at least 6 h prior to the imaging session. Prior to one of two PET imaging sessions, patients were injected intravenously with oCRH (Acthrel® 1 mcg/kg up to a maximum dose of 100 mcg) at one of three

time points: 0, 2, or 4 h prior to PET imaging. ^{18}F-FDG (10 mCi in patients ≥ 18 years, 0.08 mCi/kg in patients <18) was injected intravenously (over a period of ~1 min), 60 min before PET imaging. A transmission scan was obtained with a ^{137}Cesium rotating pin source to correct for attenuation. A cap with small light reflectors was placed on the subject's head to monitor head position during PET imaging with a Polaris Vicra head tracking system (Northern Digital Inc.). This information on head movement was utilized to reduce the blurring effect on the PET images. ^{18}F-FDG PET scan of the brain was obtained for approximately 40 minutes. Data from the Siemens HRRT scanner were reconstructed, using MOLAR [24] software, into cubic voxels 1.22 mm apart. Image intensities were normalized by the injected ^{18}F-FDG dose and the subject's lean body mass as estimated by the James method [25] using the subject's sex, height, and weight. This normalization to standard uptake value (SUV) allows for comparison within and across subjects.

Quantitative ^{18}F-FDG uptake analysis

For each subject, the images from the two PET scans were first co-registered using FLIRT [26] software to find a rigid body transform that maximized the correlation ratio, and the second image was resampled with trilinear interpolation. Regions corresponding to adenomas and normal pituitary gland were identified on PET images by co-registration with post gadolinium contrast 3D-GRE MRI sequences on Carestream Vue PACS System Version 12.1.6.1005 (Carestream Health Inc., Rochester, NY, USA). To minimize intra-patient variability due to changes in the integral blood curve, SUV values were normalized to a reference region in frontal skull of each PET image [27].

Qualitative ^{18}F-FDG uptake analysis

Two experienced, board-certified neuroradiologists (JS and NP) independently read the original and multi-planar reconstructions of high-resolution ^{18}F-FDG-PET images for this study. The neuroradiologists were blinded to MRI imaging, oCRH administration, clinical characteristics, and surgical outcomes of these subjects. Each was asked to denote whether the PET image was "negative" or "positive" for a pituitary adenoma and its location. The order of PET images ($n = 54$, two per subject) read by the neuroradiologists was randomized prior to evaluation using a random sequence generator (Random Sequence Generator, Random. com). The neuroradiologist reads were then compared with MRI of the pituitary gland, surgical findings, and histopathological findings for location concordance as previously described [28].

USP8 sequence analysis in DNA samples

DNA was extracted from paraffin-embedded and OTC-embedded human adenoma samples using DNeasy Blood and Tissue Kit (Qiagen, Germany), then PCR amplification was performed on DNA with Platinum PCR SuperMix High Fidelity (Thermo Fischer Scientific) and primers for the 14-3-3 binding motif of USP8 (Forward: 5′-CTTGACCC AATCACTGGAAC, Reverse: 5′-TTACTGTTGGCTTCC TCTTCTC). Direct sequencing of PCR products after purification was performed (Eurofins MWG, USA, and NIH CCR Genomics Core, Bethesda), and sequence alignment and comparison was performed with MacVector with Assembler (MacVector, Inc, USA).

Multiplex fluorescent immunohistochemistry (mIHC)

Multiplex fluorescence immunohistochemistry was performed on 5 μm-thick paraffin-embedded sections of surgical specimens. Sections were first deparaffinized using standard Xylene/Ethanol/Rehydration steps followed by antigen retrieval in 10 mM Tris/EDTA buffer pH 9.0. The sections were then incubated with Human BD Fc receptor Blocking solution (BD Biosciences, USA) and then incubated in True Black Reagent (Biotium, USA) to quench intrinsic tissue autofluorescence. The sections were then stained for 1 h at RT using 1–5 μg/ml cocktail mixture of the following immunocompatible primary antibodies: unconjugated mouse IgG1 anti-hexokinase 2 (Abcam), unconjugated rat IgG2a anti-EGFR (GeneTex), unconjugated sheep IgG anti-GLUT1 (Abcam), Alexa Fluor 488-conjugated rabbit IgG anti-LDHA (Novus Biologicals), CF594-conjugated rabbit IgG anti-phospho EGFR Tyr992 (Cell Signaling, Biotium) and Alexa Fluor 647-conjugated rabbit IgG anti-PFKFB3 (Abcam). Following a wash in PBS supplemented with 1 mg/ml bovine serum albumin (BSA), tissue bound unconjugated antibodies were stained using a 1 μg/ml mixture of the appropriately cross-adsorbed secondary antibodies (Thermo Fisher, Li-Cor Biosciences) conjugated to spectrally compatible fluorophores (Alexa Fluor 430, Alexa Fluor 546, IRDye 680LT). Sections were counterstained using 1 μg/ml DAPI (Thermo Fisher) for visualization of cell nuclei. Slides were imaged using a multi-channel wide field epifluorescence microscope and images were acquired from whole specimen sections using the Axio Imager.Z2 slide scanning fluorescence microscope (Zeiss) equipped with a 20×/0.8 Plan-Apochromat (Phase-2) non-immersion objective (Zeiss), a high-resolution ORCA-Flash4.0 sCMOS digital camera (Hamamatsu), a 200 W X-Cite 200DC broad band lamp source (Excelitas Technologies), and seven customized filter sets to image the aforementioned fluorophores with minimal spectral cross-talk (Semrock). Pseudocolored stitched images were then exported to Adobe Photoshop and overlaid as individual layers to create multicolored merged composites.

Location of the adenoma

The final assignment of the true location of adenoma was based on the histopathology reports. In instances of multiple specimens obtained during a procedure, the true location of the adenoma was assigned based on the original site of the specimen containing the adenoma.

Statistical analysis

The results are reported as mean ± standard deviation (SD) or 95% confidence intervals (95% CI). Paired t-test analysis was performed to measure differences under test/re-test conditions. Statistical differences between groups were compared using one-way ANOVA with Holmes-Sidak correction for multiple comparisons. Statistical analysis of contingency tables and binary variables were performed using Chi-squared test. Statistical significance was set at $p < 0.05$ (with Bonferroni corrections when multiple statistical tests were run).

Results

Thirty subjects were recruited to the study, of which, three subjects (subject #0, 5, and 24) were withdrawn due to subject preference, inability to obtain a reliable intravenous catheter for oCRH administration, and unavailability of oCRH, respectively (Fig. 1). Twenty-seven subjects (20 females and 7 males) were included (mean age 34.9 ± 16.8 years; range 10–61 years). Four of the 27 patients presented with recurrent CD (Table 1). Following completion of research procedures (two ^{18}F-FDG-PET scans), all subjects underwent standard-of-care transsphenoidal surgery for
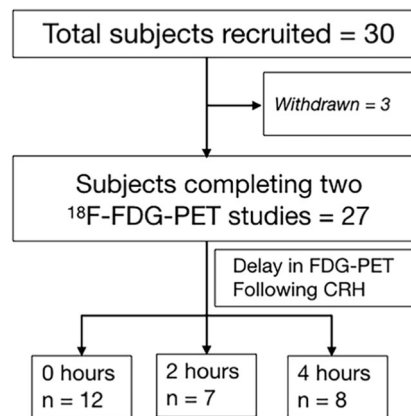

Fig. 1 Study summary

Table 1 Summary statistics

Sub No.	Age, Sex	CD Diagnosis	MRI	Size (mm)	Delay (h)	^{18}F-FDG-PET	CRH + ^{18}F-FDG-PET
1	15, F	New	−	−	0	−	−
2	37, F	New	+	12	0	+	+
3	13, M	New	?	−	0	−	−
4	15, M	New	+	4	0	−	−
6	37, F	Recurrent	?	−	0	−	−
7	58, F	New	+	3	0	+	+
8	15, F	New	−	3	0	−	−
9	48, F	New	+	4	0	−	−
10	44, M	Recurrent	−	−	0	−	+
11	50, F	New	+	14	0	+	+
12	11, M	New	?	−	0	−	−
13	40, F	New	+	10	0	−	−,+
14	61, F	New	−	−	2	+	+
15	42, F	New	+	12	2	−,+	−, +
16	35, F	New	+	2.8	2	−	−
17	51, F	New	+	15	2	−	+
18	60, F	New	+	7	2	+	+
19	51, F	New	−	−	2	−	−
20	12, M	New	+	1.3	2	−, +	+
21	46, F	New	+	5	4	−	+
22	18, F	Recurrent	+	7	4	+	+
23	52, M	New	+	16	4	−, +	+
25	34, F	New	+	10	4	+	+
26	10, F	New	+	7	4	−, **±**	**±**, −
27	25, M	Recurrent	?	−	4	−	−
28	40, F	New	+	6	4	+	+
29	22, F	New	+	18	4	−	−

Subjects are numbered according to the study convention. Age at study accrual is presented in years. The diagnosis of Cushing's disease (CD) was based on clinical and biochemical data, supported by clinical standard of care MRI of the pituitary gland with gadolinium contrast. Recurrence and clinical MRI results are represented. The maximum diameter of distinct adenomas detected on MRI are presented in millimeters. Delay in administering ^{18}F-FDG following oCRH stimulation is shown in hours. Blinded neuroradiologist reads of ^{18}FDG-PET images are shown in the last two columns. Positive or absent adenoma detection by neuroradiologists is denoted by " +" and "−" respectively. Consensus reads are presented with one symbol. Bolded " +" symbols represent detection of adenomas not visible on baseline PET imaging, but visible with CRH stimulation. A disagreement in reads is presented as different symbols in the order of neuroradiologist reads (JS, then NP). Subjects 5, 24, and 30 withdrew from the study. Subjects 10 and 14 had MRI negative adenomas that were detected on FDG-PET imaging

resection of corticotropinoma. Histological examination of resected specimens confirmed pituitary adenomas with a positive ACTH immunostain in all cases. Pre-operative MRI imaging detected distinct adenomas in 20 (68%) cases. In the rest, the imaging was either read as negative ($n = 5$) or questionable ($n = 4$) for a pituitary adenoma (Table 1).

Quantitative ^{18}F-FDG uptake

The a priori primary outcome measure of the study was to determine the effect of CRH stimulation on ^{18}F-FDG uptake in adenomas. The mean SUV (SUV_{Mean}) of adenomas significantly increased from baseline (3.6 ± 1.5) with oCRH administration (3.9 ± 1.7; one tailed $p = 0.003$; mean difference = 0.3; 95% CI 0.1–0.6). The maximum SUV (SUV_{Max}) of adenomas, however, did not change significantly from baseline with oCRH administration (SUV_{Max} 5.5 ± 3.7 to 5.6 ± 3.3 respectively, $p = 0.3$) (Fig. 2). Congruent with laboratory findings [21], neither the SUV_{Mean} nor SUV_{Max} was significantly affected by CRH stimulation in the regions corresponding to the adjacent normal pituitary gland, suggesting a selective effect of oCRH on corticotropinoma ^{18}F-FDG uptake. The SUV_{Mean} or SUV_{Max} of adenomas following delayed scans (2-h

Fig. 2 CRH stimulation results in elevated SUV in adenomas. Mean of SUV **a** and maximum of SUV **c** are depicted in this pairwise analysis. The y-axis depicts the change in the SUV measure of the adenoma. The dot plots demonstrate the residuals (differences) between CRH stimulated and baseline PET mean adenoma SUV **b** and maximum adenoma SUV **d**. In all the panels, adenomas detected as a consensus by neuroradiologists have been highlighted in red. CRH corticotropin releasing hormone, FDG-PET ^{18}F-FDG-PET at baseline, CRH+FDG-PET ^{18}F-FDG-PET with oCRH stimulation, SUV standardized uptake values. $*p \leq 0.05$
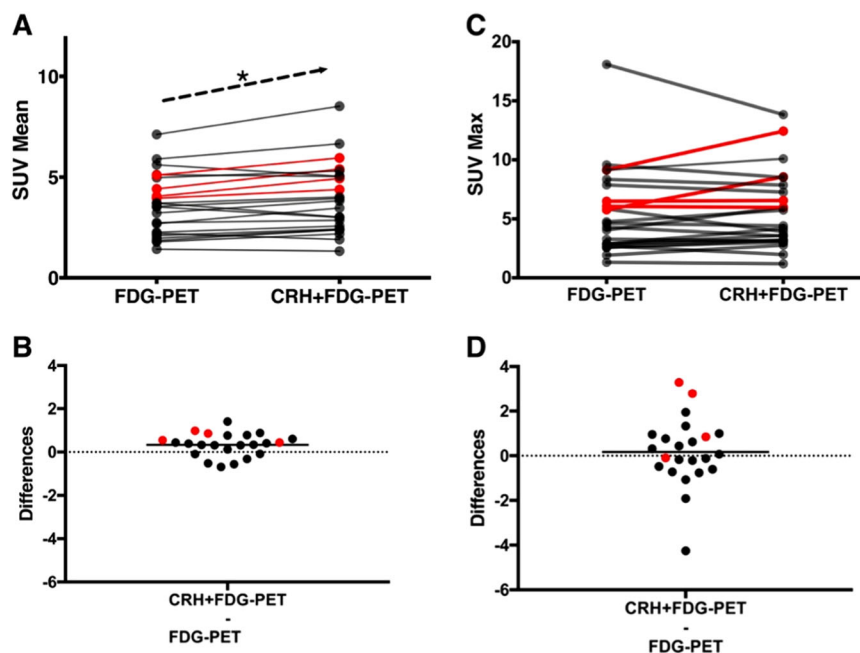
Fig. 3 MRI Negative adenomas are detected with baseline and CRH stimulated FDG-PET imaging. In five subjects (including Subjects 14 and 10), MRI of the pituitary gland was negative (**a** and **d**). In Subject 14, a histopathologically confirmed adenoma was visible (white arrowhead) on baseline **b** and CRH stimulated FDG-PET imaging **c**. In Subject 10, baseline FDG-PET imaging **e** failed to demonstrate an adenoma. A distinct adenoma within the left cavernous sinus was visible (white arrowhead) upon CRH stimulated FDG-PET imaging **f**
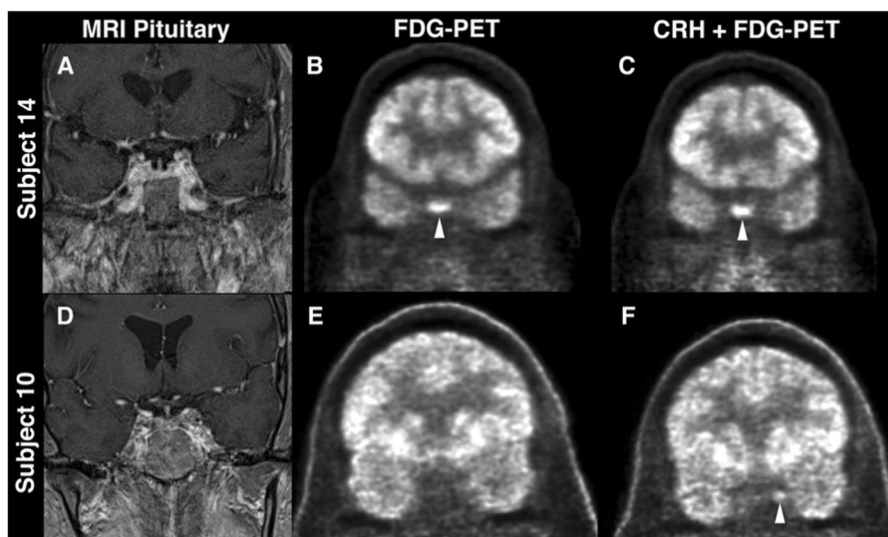
delayed and 4-h delayed) was unchanged from those performed when oCRH was given with ^{18}F-FDG.

Qualitative ^{18}F-FDG-PET findings

A secondary outcome measure of the study addressed the clinical utility of oCRH stimulated ^{18}F-FDG-PET imaging to identify corticotropinoma. Of the 54 ^{18}F-FDG-PET images read (oCRH and non-oCRH image for each patient), neuroradiologists agreed that pituitary adenomas were visible ("positive") on 21 scans, not visible ("negative") on 26 scans, and disagreed on the findings of 7 scans. Overall, the inter-rater agreement between the neuroradiologist reads was 'good' [29] with kappa = 0.7 (SE of kappa

= 0.08, 95% CI 0.6–0.9) (Table 1). There were no false positive reads by adenoma location. The recorded location of the adenomas on PET images by the neuroradiologists corresponded with the location confirmed by histopathological examination. PET following oCRH administration detected 15 of 27 adenomas and McNemar's test revealed statistically significant correlation for one radiologist reading with use of oCRH for detection of adenomas (NP: one tailed $p = 0.02$; JS: one tailed $p = 0.2$).

In all cases (except subject 26 for one neuroradiologist), adenomas detected on baseline PET images were also detected upon oCRH stimulation as well. Importantly, both neuroradiologists reported an increase in ^{18}F-FDG-PET detection of adenomas following CRH administration

Table 2 Effect of delay in PET imaging following CRH stimulation

Neuroradiologist	Number of corticotropinomas detected				Chi Square for trend
	0 h	2 h	4 h	Overall	P value
1	1/9 (11%)	2/5 (40%)	3/5 (60%)	6/19 (32%)	0.05
2	2/9 (22%)	1/3 (33%)	1/3 (33%)	4/15 (27%)	0.66

The column titles illustrate the delay in ^{18}F-FDG administration following oCRH stimulation (in hours). The denominators at each time point represent the number of FDG PET negative tumors read by the neuroradiologist. The numerator represents the positive tumors detected within this cohort following CRH administration. We found no trends of increased detection (Chi square for trend) of adenomas by either blinded neuroradiologists (rows 1 and 2). Of the 19 adenomas not detected on baseline PET imaging, oCRH stimulation resulted in detection of 6 and 3 additional adenomas (column – Overall)

Table 3 Summary of statistics for corticotropinomas detected on baseline and oCRH stimulated ^{18}F-FDG-PET

Variable	Baseline PET			CRH stimulated PET		
	Negative	Positive	p value	Negative	Positive	p value
Age (years)	31.2 ± 15.2	44.8 ± 15.2	0.18	26.1 ± 14.4	43.3 ± 15.2	0.04
Sex (female/male)	10/5	8/0	0.07	7/4	10/3	0.48
SUV Max	3.5 ± 1.8	9.0 ± 4.5	<0.0001[†]	3.0 ± 1.0	7.5 ± 2.7	0.0005[†]
SUV Mean	2.7 ± 1.0	5.0 ± 1.3	0.0002[†]	2.6 ± 0.8	5.1 ± 1.6	<0.0001[†]
Serum ACTH MN (pg/ml)	49.7 ± 75.2	62.6 ± 45.2	0.73	28.1 ± 17.5	111.8 ± 86.7	0.02
Serum ACTH AM (pg/ml)	39.7 ± 31.04	91.05 ± 62.6	0.15	29.8 ± 16.7	116.7 ± 85.9	0.01
Serum ACTH w/CRH (%)	391.9 ± 257.5	262.3 ± 156.3	0.32	362.1 ± 209.8	289.1 ± 163.9	0.67
Serum Cortisol MN (mg/dl)	16.8 ± 12.1	20.4 ± 6.0	0.82	14.8 ± 8.5	26.0 ± 19.6	0.11
Serum Cortisol AM (mg/dl)	19.2 ± 11.1	23.87 ± 8.1	0.76	17.7 ± 10.7	30.3 ± 21.4	0.09
Serum Cortisol w/CRH (%)	199.2 ± 65.7	131.5 ± 20.8	0.01	203.3 ± 68.6	128.4 ± 18.8	0.004[†]

AM morning, *MN* midnight

[†]Statistically significant following Bonferroni correction (adjusted $p \leq 0.007$)

(Fig. 3). NP correctly detected the adenoma on 8/27 baseline PET scans and in 6 additional cases (14/27) with oCRH stimulation. JS correctly detected the adenoma in 12/27 baseline scans and in 3 additional cases (15/27) with CRH stimulation. There was no statistically significant increase in detection of adenomas by either neuroradiologists by introducing a delay in PET imaging following CRH administration (Chi Square for trend, NP: $p = 0.05$; JS: $p = 0.66$,) (Table 2). Readings from Subject 26 were diametrically opposite and conflicting, and therefore excluded from further analysis (Table 1). Interestingly, in two cases, adenomas initially read as MRI negative were detected on PET imaging by both neuroradiologists (Subjects 10 and 14). In Subject 10, the adenoma was only detected following administration of oCRH (Table 1 and Fig. 3).

We then analyzed the ^{18}F-FDG uptake characteristics of adenomas detected by neuroradiologists. For this analysis, we only included adenomas with consensus reads between both the study neuroradiologists (47/54 studies). As we have reported earlier [3], we found a significantly higher SUV$_{Mean}$ (5.0 ± 1.3 vs. 2.7 ± 1.0; $p < 0.001$) and SUV$_{Max}$ (9.0 ± 4.5 vs. 3.5 ± 1.8; $p < 0.001$) in adenomas detected by the neuroradiologists on baseline ^{18}F-FDG-PET scans (Table 3), compared to values in adenomas that were not detected. Higher SUV$_{Mean}$ (5.1 ± 1.7 vs. 2.6 ± 0.8; $p < 0.001$) and SUV$_{Max}$ (7.5 ± 2.7 vs. 3.0 ± 0.9; $p < 0.001$) was also measured in adenomas detected following oCRH stimulation (Fig. 4). There was no apparent effect of size on FDG PET detection of adenomas. Adenomas as small as 1.3 mmm and 3 mm were detected in PET imaging. However, PET imaging failed to detect some larger adenomas (Subject 29, 18 mm) as well (Table 1).

Among the six adenomas that were detected only upon oCRH stimulation, five demonstrated increased SUV$_{Mean}$ (24.17% ± 26.2%, range: 6.76% –70.33%). SUV$_{Mean}$ of the adenomas was increased from 3.6 ± 1.3 to 4.2 ± 0.9 (one tailed $p = 0.03$) with oCRH stimulation (Fig. 4). However, overall, there was no statistically significant increase in the SUV$_{Max}$ of adenomas with oCRH stimulation ($p = 0.13$). Taken together, these findings suggest that oCRH

Fig. 4 Adenomas detected on PET images have higher SUV. Mean of SUV **a** and maximum of SUV **b** were higher in adenomas detected (+) when compared with those undetected (−) on PET imaging. This relationship was observed on both baseline ^{18}F-FDG-PET studies (FDG-PET) and those following oCRH stimulation (CRH+FDG-PET). In those adenomas detected only following CRH stimulation, we found a significant increase in mean SUV **c**, but no trend in the maximum SUV (D). CRH: corticotropin releasing hormone; FDG-PET: ^{18}F-FDG-PET at baseline; CRH+FDG-PET: ^{18}F-FDG-PET with oCRH stimulation; SUV: standardized uptake values; *$p \leq 0.05$; ***$p \leq 0.001$; ****$p \leq 0.0001$
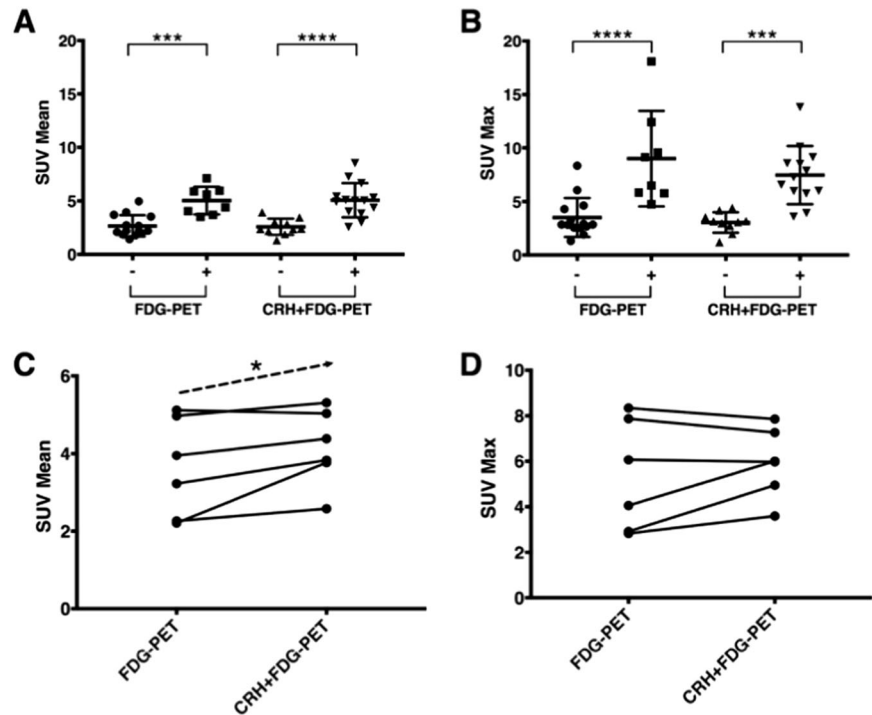
Fig. 5 Corticotropinomas express hexokinase 2 and lactate dehydrogenase A. Paraffin embedded surgical tissues were examined with hematoxylin and eosin stain to confirm adenoma **a**. Upon multiplexed immunohistochemical staining, adenomas (*) overexpressed lactate dehydrogenase A **b** and hexokinase 2 **c** compared to the normal pituitary gland (●). The merged images demonstrate significant overlap of lactate dehydrogenase A and hexokinase 2 within the adenoma **d**
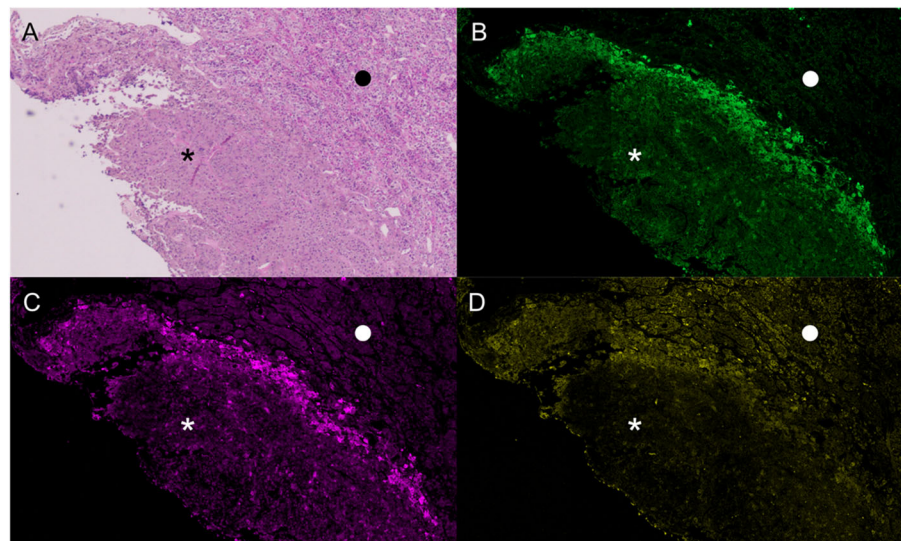
stimulation may lead to an increased mean ^{18}F-FDG uptake selectively within the adenoma and, consequently, to more frequent adenoma detection by neuroradiologists.

Factors associated with ^{18}F-FDG-PET detection of adenomas

We tested whether age, sex, size of the adenoma, presence of invasion, plasma ACTH level, serum cortisol level, and percentage change in ACTH/cortisol level following oCRH stimulation were associated with detection of adenomas on

PET imaging, setting the significance level at $p = 0.05/7 = 0.007$ (Bonferroni correction). An association was only found with a lower percentage of rise in serum cortisol of adenomas detected compared to those not detected (128% vs. 203%; mean difference 75%, 95% CI 23–127%) during oCRH stimulation (adjusted $p = 0.004$) (Table 3). This is similar to our prior findings in baseline PET studies [3]. These findings suggest that adenomas detected on oCRH stimulated PET images may be closer to maximal hormone secretion prior to stimulation, leading to increased energy substrate demand and ^{18}F-FDG uptake.

On available paraffin embedded histopathological sections ($n = 17$), we performed multiplexed immunohistochemistry staining to probe for important proteins in the glycolytic pathway. We found that adenomas ubiquitously expressed GLUT1, as well as isozymes hexokinase 2 and lactate dehydrogenase A (Fig. 5). We did not find an association with the intensity of immunohistochemical staining with either SUV$_{Max/Mean}$ or neuroradiology reads of corticotropinomas. We also did not detect a difference between *USP8*-mutant and *USP8*-wildtype corticotropinomas in SUV or neuroradiology reads.

Discussion

The theoretical underpinnings of ^{18}F-FDG-PET use were established in early studies that showed little net oxidation of glucose by either the Krebs' cycle or the pentose phosphate pathway in the normal pituitary gland. Non-esterified fatty acids were recognized as the main energy substrates for normal pituitary cells [30, 31]. However, ^{18}F-FDG PET results hinted at metabolic reprogramming of pituitary adenomas to rely on glycolysis as the primary energy source, similar to the Warburg effect in malignant tumors [32, 33]. In large observational studies of whole body ^{18}F-FDG-PET studies, incidental sellar ^{18}F-FDG uptake was found in less than 1% of cases, and this sign was highly specific for the presence of pituitary adenomas [17–19]. Although highly specific [17–19], sellar ^{18}F-FDG uptake remains a relatively insensitive (~40%) marker for pituitary adenomas [3, 20].

Pituitary microadenomas detected on PET imaging demonstrate elevated SUV values when compared with the undetected adenomas [3]. Here, we first asked whether modulation of ^{18}F-FDG uptake (to elevate SUV) in corticotropin secreting adenomas is possible with secretagogue stimulation. Previous work indicates that such modulation of ^{18}F-FDG uptake is possible. Secretagogues further stimulate glucose uptake in hormone secreting cells such a pituitary gonadotrophs and thyroid follicle cells [34, 35]. Conversely, treatment of prolactin or growth hormone secreting pituitary macroadenomas with bromocriptine or somatostatin analogues reduces ^{18}F-FDG uptake [36].

When we demonstrated that in vitro CRH stimulation selectively increases glucose uptake in human derived corticotropinoma cells, there was no direct clinical evidence supporting a similar effect in vivo. In a small study of 5 subjects with CD, human CRH (100 mcg) and ^{18}F-FDG were co-administered, followed by PET-CT image acquisition 60 min later. In this study, no increase in SUV$_{Max}$ of the pituitary region was detected [37]. Consistent with these findings, in the larger current study, we found no change in the SUV$_{Max}$ in corticotropinoma after oCRH stimulation. However, we did find a significant increase in the SUV$_{Mean}$ in corticotropinoma with oCRH. Additionally, we found no change in ^{18}F-FDG uptake characteristics, including change in SUV$_{Mean}$, in normal pituitary gland after oCRH stimulation. These findings suggest a selective effect of oCRH stimulation on the increase in SUV$_{Mean}$ of adenoma. Although adenomas with higher SUV$_{Max}$ were detected by neuroradiologists, we found a larger effect of SUV$_{Mean}$ on the detection rate. This selective effect of oCRH underlies the increased rate of detection (44% to 55%) of corticotropinomas on PET images by blinded neuroradiologists in our study. Importantly, the neuroradiologists did not report any false positive readings in PET images.

Ultimately, the role of FDG-PET imaging in CD would likely be as a complementary imaging modality. In this study, we found that in two of the five tumors read as negative on clinical MRI scans, adenomas were detected on PET imaging. In one of these instances, the adenoma was detected only after oCRH stimulation, suggesting a complementary role for FDG-PET imaging following secretagogue stimulation in MRI negative cases of CD. The size of adenomas (on MRI of the pituitary gland) does not appear to be associated with increased detection on FDG-PET imaging. A valuable property of ^{18}F-FDG-PET in our study was the absence of false positive reads. In actual clinical practice, in many instances, MRI findings of adenomas are uncertain. We believe that in such instances, oCRH-stimulated ^{18}F-FDG-PET imaging may help clinicians localize the adenoma pre-surgically.

Initially, the current protocol was designed with simultaneous administration of oCRH and ^{18}F-FDG. This schema allowed for about 45-min delay between oCRH administration and image acquisition. There is strong evidence for delayed (2–4 h) increase in glucose uptake in hormone secreting cells following secretagogue stimulation, suggesting that a longer delay might result in a greater effect [21, 34, 35]. However, modification of the study to incorporate a two or four hour delay in ^{18}F-FDG administration following oCRH infusion, did not reliably increase SUV or neuroradiologist detection of adenomas.

We found that the corticotropinomas detected on oCRH stimulated FDG-PET imaging had previously demonstrated a lower rise in serum cortisol at 30 and 45 min during oCRH stimulation testing. We also found a trend towards higher plasma midnight and morning ACTH in these adenomas (Table 3). These findings suggest that the corticotropinomas with elevated hormone secretion were near maximal hormone secretion and metabolically more active. Interestingly, we found that corticotropinomas ubiquitously expressed markers of metabolic reprogramming such as GLUT1, HK2, and LDHA (Fig. 5). Prior studies of

malignant human tumors have reported on the association between such markers and FDG-PET detection. However, we found ubiquitous expression of these markers in corticotropinomas. We suspect that unlike malignant tumors carrying multiple mutations and epigenetic derangements, corticotropinomas lack a heterogenous range of expression of such markers. Within the range of expression of such markers, we did not find an association with ^{18}F-FDG uptake in corticotropinomas. While others reported that USP8 mutations in the 14-3-3 binding region lead to enhanced EGF signaling in corticotropinomas [38, 39], we did not find an effect on ^{18}F-FDG uptake.

We envision the true utility of ^{18}F-FDG-PET imaging for detecting pituitary microadenomas to be complementary to the current MRI diagnostic strategy. This study suggests increased detection of corticoptropinomas utilizing oCRH stimulation on PET detection, therefore, a follow up study is being designed to explore the effect of oCRH stimulation on PET detection of MRI invisible corticotropinomas. The HRRT system is a high-resolution, dedicated human brain PET scanner that is not widely available for clinical use [40, 41]. The detection rate of microadenomas causing CD is similar to other studies using widely available PET-CT platforms [4, 20, 37]. This suggests that the results of this study may be generalizable for clinical imaging. In the current study, patients received minimal radiation activity of up to 10 mCi for adults and 0.08 mCi/Kg for children with a maximum of 6.3 mCi through ^{18}F-FDG administration. We also recognize that the additional costs associated with HRRT PET imaging were not addressed here in this study.

Conclusions

The current study suggests that oCRH stimulation may lead to increased ^{18}F-FDG uptake, and increased rate of detection of corticotropinomas in CD. These findings invite further prospective evaluation of oCRH stimulated ^{18}F-FDG-PET imaging of MRI invisible adenomas causing CD. If validated, oCRH stimulated PET imaging could complement MRI to improve pre-surgical visualization of ACTH secreting microadenomas.

Compliance with ethical standards

References

1. D. Bochicchio, M. Losa, M. Buchfelder, Factors influencing the immediate and late outcome of Cushing's disease treated by transsphenoidal surgery: a retrospective study by the European Cushing's Disease Survey Group. J. Clin. Endocrinol. Metab. **80**, 3114–3120 (1995)

2. T. Moshang, Editorial: Cushing's disease, 70 years later… and the beat goes on. J. Clin. Endocrinol. Metab. **88**, 31–33 (2003)

3. P. Chittiboina, B.K. Montgomery, C. Millo, P. Herscovitch, R.R. Lonser, High-resolution 18 F-fluorodeoxyglucose positron emission tomography and magnetic resonance imaging for pituitary adenoma detection in Cushing disease. J. Neurosurg. **122**, 1–7 (2014)

4. I.N. Chowdhury, N. Sinaii, E.H. Oldfield, N. Patronas, L.K. Nieman, A change in pituitary magnetic resonance imaging protocol detects ACTH-secreting tumours in patients with previously negative results. Clin. Endocrinol. **72**, 502–506 (2010)

5. D.A. Finelli, B. Kaufman, Varied microcirculation of pituitary adenomas at rapid, dynamic, contrast-enhanced MR imaging. Radiology **189**, 205–210 (1993)

6. R. Kasaliwal, S.S. Sankhe, A.R. Lila, S.R. Budyal, V.S. Jagtap, V. Sarathi et al. Volume interpolated 3D-spoiled gradient echo sequence is better than dynamic contrast spin echo sequence for MRI detection of corticotropin secreting pituitary microadenomas. Clin. Endocrinol. **78**, 825–830 (2013)

7. R.R. Lonser, J.J. Wind, L.K. Nieman, R.J. Weil, H.L. DeVroom, E.H. Oldfield, Outcome of surgical treatment of 200 children with Cushing's disease. J. Clin. Endocrinol. Metab. **98**, 892–901 (2013)

8. W.W. de Herder, P. Uitterlinden, H. Pieterman, H.L. Tanghe, D.J. Kwekkeboom, H.A. Pols et al. Pituitary tumour localization in patients with Cushing's disease by magnetic resonance imaging. Is there a place for petrosal sinus sampling? Clin. Endocrinol. **40**, 87–92 (1994)

9. E.H. Oldfield, J.L. Doppman, L.K. Nieman, G.P. Chrousos, D.L. Miller, D.A. Katz et al. Petrosal sinus sampling with and without corticotropin-releasing hormone for the differential diagnosis of Cushing's syndrome. N. Engl. J. Med. **325**, 897–905 (1991)

10. J.J. Wind, R.R. Lonser, L.K. Nieman, H.L. DeVroom, R. Chang, E.H. Oldfield, The lateralization accuracy of inferior petrosal sinus sampling in 501 patients with Cushing's disease. J. Clin. Endocrinol. Metab. **98**, 2285–93 (2013)

11. J. Jagannathan, R. Smith, H.L. DeVroom, A.O. Vortmeyer, C.A. Stratakis, L.K. Nieman, et al. Outcome of using the histological pseudocapsule as a surgical capsule in Cushing disease. J. Neurosurg. **111**, 531–9 (2009).

12. E.H. Oldfield, Surgical management of Cushing's disease: a personal perspective. Clin. Neurosurg. **58**, 13–26 (2011)

13. E.H. Oldfield, A.O. Vortmeyer, Development of a histological pseudocapsule and its use as a surgical capsule in the excision of pituitary tumors. J. Neurosurg. **104**, 7–19 (2006)

14. M. Bergström, C. Muhr, K. Ericson, H. Lundqvist, A. Lilja, L. Eriksson et al. The normal pituitary examined with positron emission tomography and (methyl-11C)-L-methionine and (methyl-11C)-D-methionine. Neuroradiology **29**, 221–225 (1987)

15. B. De Souza, A. Brunetti, M.J. Fulham, R.A. Brooks, D. DeMichele, P. Cook et al. Pituitary microadenomas: a PET study. Radiology **177**, 39–44 (1990)

16. S.H. Hyun, J.Y. Choi, K.-H. Lee, Y.S. Choe, B.-T. Kim, Incidental focal ^{18}F-FDG uptake in the pituitary gland: clinical significance and differential diagnostic criteria. J. Nucl. Med. **52**, 547–50 (2011)

17. S.Y. Jeong, S.-W. Lee, H.J. Lee, S. Kang, J.-H. Seo, K.A. Chun et al. Incidental pituitary uptake on whole-body ^{18}F-FDG PET/CT: a multicentre study. Eur. J. Nucl. Med. Mol. Imaging **37**, 2334–43 (2010)

18. H. Ju, J. Zhou, Y. Pan, J. Lv, Y. Zhang, Evaluation of pituitary uptake incidentally identified on ^{18}F-FDG PET/CT scan. Oncotarget **8**, 55544–55549 (2017)

19. C.W. Koo, P. Bhargava, V. Rajagopalan, M. Ghesani, H. Sims-Childs, N.J. Kagetsu, Incidental detection of clinically occult pituitary adenoma on whole-body FDG PET imaging. Clin. Nucl. Med. **31**, 42–3 (2006)

20. A.S. Alzahrani, R. Farhat, A. Al-Arifi, N. Al-Kahtani, I. Kanaan, M. Abouzied, The diagnostic value of fused positron emission tomography/computed tomography in the localization of adrenocorticotropin-secreting pituitary adenoma in Cushing's disease. Pituitary **12**, 309–14 (2009)

21. J. Lu, B.K. Montgomery, G.P. Chatain, A. Bugarini, Q. Zhang, X. Wang et al. Corticotropin releasing hormone can selectively stimulate glucose uptake in corticotropinoma via glucose transporter 1. Mol. Cell Endocrinol. **470**, 1–10 (2017)

22. L.K. Nieman, B.M.K. Biller, J.W. Findling, J. Newell-Price, M.O. Savage, P.M. Stewart et al. The diagnosis of Cushing's syndrome: an Endocrine Society Clinical Practice Guideline. J. Clin. Endocrinol. Metab. **93**, 1526–40 (2008)

23. N. Patronas, N. Bulakbasi, C.A.A. Stratakis, A. Lafferty, E.H.H. Oldfield, J. Doppman et al. Spoiled gradient recalled acquisition in the steady state technique is superior to conventional postcontrast spin echo technique for magnetic resonance imaging detection of adrenocorticotropin-secreting pituitary tumors. J. Clin. Endocrinol. Metab. **88**, 1565–1569 (2003)

24. R.E. Carson, W.C. Barker, J.-S.L.J.-S. Liow, C.A. Johnson, Design of a motion-compensation OSEM list-mode algorithm for resolution-recovery reconstruction for the HRRT. 2003 IEEE NSS/MIC Conf. Rec. **5**:3281–3285 (2003)

25. DHSS/MRC Group on Obesity Research., James WPT (William PT, Waterlow JC (John C: Research on Obesity: A Report of the DHSS/MRC Group. H.M.S.O, 1976

26. M. Jenkinson, S. Smith, A global optimisation method for robust affine registration of brain images. Med. Image Anal. **5**, 143–56 (2001)

27. B. Bai, J. Bading, P.S. Conti, Tumor quantification in clinical positron emission tomography. Theranostics **3**, 787–801 (2013)

28. G.P. Chatain, N. Patronas, J.G. Smirniotopoulos, M. Piazza, S. Benzo, A. Ray-Chaudhury, et al. Potential utility of FLAIR in MRI-negative Cushing's disease. J. Neurosurg. **129**, 1–9 (2017)

29. D.G. Altman, Practical Statistics for Medical Research. London: Chapman and Hall (1991)

30. F. Maher, S.J. Vannucci, I.A. Simpson, Glucose transporter proteins in brain. FASEB J. **8**, 1003–1011 (1994)

31. J.R. Viña, R.B. Page, D.W. Davis, R.A. Hawkins, Aerobic glycolysis by the pituitary gland in vivo. J. Neurochem. **42**, 1479–82 (1984)

32. M.G.Vander Heiden, L.C. Cantley, C.B. Thompson, P. Mammalian, C. Exhibit, Metabolism A: understanding the Warburg Effect: cell proliferation. Science **324**, 1029–1034 (2009)

33. O. Warburg, Injuring of respiration the origin of cancer cells. Science **123**, 309–14 (1956)

34. S. Filetti, G. Damante, D. Foti, Thyrotropin stimulates glucose transport in cultured rat thyroid cells. Endocrinology **120**, 2576–81 (1987)

35. V.M. Harris, S.V. Bendre, F. Gonzalez De Los Santos, A. Fite, A. El-Yaman El-Dandachli, L. Kurenbekova et al. GnRH increases glucose transporter-1 expression and stimulates glucose uptake in the gonadotroph. J. Endocrinol. **212**, 139–147 (2012)

36. T.L. Francavilla, R.S. Miletich, D. DeMichele, N.J. Patronas, E.H. Oldfield, B.D. Weintraub et al. Positron emission tomography of pituitary macroadenomas: hormone production and effects of therapies. Neurosurgery **28**, 826–833 (1991)

37. H.P. Patt, V. Lele, A. Lila, T. Bandgar, N. Shah, Utility of hCRH-stimulated (18) F-FDG PET-CT scan in localisation of pituitary microadenoma in Cushing's disease. J. Med. Imaging Radiat. Oncol. **58**, 213 (2014)

38. Z.-Y. Ma, Z.-J. Song, J.-H. Chen, Y.-F. Wang, S.-Q. Li, L.-F. Zhou et al. Recurrent gain-of-function USP8 mutations in Cushing's disease. Cell Res. **25**, 306–317 (2015)

39. M. Reincke, S. Sbiera, A. Hayakawa, M. Theodoropoulou, A. Osswald, F. Beuschlein et al. Mutations in the deubiquitinase gene USP8 cause Cushing's disease. Nat. Genet. **47**, 31–38 (2014)

40. H.Wa.M. de Jong, F.H.P. van Velden, R.W. Kloet, F.L. Buijs, R. Boellaard, A. Lammertsma, a: Performance evaluation of the ECAT HRRT: an LSO-LYSO double layer high resolution, high sensitivity scanner. Phys. Med. Biol. **52**, 1505–26 (2007)

41. F.H.P. van Velden, R.W. Kloet, B.N.M. van Berckel, F.L. Buijs, G. Luurtsema, A. Lammertsma, et al. HRRT versus HR+ human brain PET studies: an interscanner test-retest study. J. Nucl. Med. **50**, 693–702 (2009)